Stretched Sensing Strategies for IEPE

Łukasz Huchel, Thomas C. Krause, Steven B. Leeb, *Fellow, IEEE*, and Jan Helsen

***Abstract*— The integrated electronics piezoelectric (IEPE) standard is a common interfacing strategy for industrial accelerometers that are used for vibration and acoustic measurements. The IEPE interface is an untapped resource with opportunities for expanded sensing, including measurements with frequency content down to dc such as temperature or pressure. This article proposes a new IEPE-compatible transducer, built around an embedded acquisition device, which supports a wide range of sensing elements. The proposed system stretches the range of applications for the IEPE interface. In addition, an inexpensive IEPE-compatible microphone is presented, with detailed modeling and experimental verification. A discussion of a condition monitoring system and strategy highlights the benefits of the proposed hardware.**

***Index Terms*— Condition monitoring, current loop sensing, industry 40, integrated electronics piezoelectric (IEPE), Internet of Things (IoT).**

I. INTRODUCTION

ADVANCES in the deployment of cyber-physical devices or "Internet of Things" (IoT) devices are heralded as the "Fourth Industrial Revolution" and "Industry 4.0," akin to previous human progress due to steam, electricity, and early computers [1]–[3]. To fully realize the potential of the IoT for monitoring and diagnostics, quality, not quantity, of data must be the priority for system designers [4]–[6]. For example, a generic current loop vibration sensor may be easy to install but prove to be of little value if bandwidth, frequency limits, or quantization prevent the collection of useful information. Even just one "good" sensor, e.g., a piezoelectric-based accelerometer, that provides an information-rich stream of actionable data that can be mined with signal processing algorithms may be worth considerably more than a collection of inexpensive or easily manufactured, but limited, sensors.

Current loop signal transmission is a workhorse for industrial process control [7]. Current loops allow for reliable transmission of process variable (PV) data. The transmission of voltage signals over long two-wire channels is unreliable due to significant voltage drops along the line and electromagnetic interference (EMI) introduced by harsh industrial environments. High-noise immunity, long-distance transmission, and the availability of a shared power and signal path over the same two wires are some of the features that have made the 4–20-mA current loop a *de facto* industrial standard. Current loops do more than just transmit PVs. A current signal is often used as a control signal. For example, current loops have gradually replaced the legacy 3–15-psi pneumatic control signal standard. Several modifications have been applied to the standard current loop, including, for instance, the Highway Addressable Remote Transducer Protocol (HART), which provides a means for digital communication over a two-wire current loop [8]. A wide range of industrial equipment is compatible with current loops due to the versatile nature of the system.

A significant application of current loops is to interface with piezoelectric-based accelerometers. There are two types of piezoelectric accelereometers: charge- and voltage-mode accelerometers [9]. Charge-mode sensors are characterized by flexible electrical parameters, a wide range of operating temperatures, wide dynamic range, and compatibility with remote amplifiers [10]. Remote analog front ends for charge-mode sensors are characterized by high impedance. Thus, they are susceptible to noise and require extra measures, such as a low-noise cabling [11]. These limitations make the charge-mode architecture more common in laboratory conditions. In contrast, voltage-mode sensors, also called low-impedance voltage mode sensors, have built-in electronics that can make them less susceptible to noise [12]. Voltage mode sensors commonly operate from a constant-current source over a two-wire interface such as a coaxial cable. The two-wire interface enables simultaneous power delivery to the sensing element and analog signal transmission [10].

Several accelerometer manufacturers use a proprietary name for the voltage mode architecture; however, the name "integrated electronics piezoelectric (IEPE)" is commonly accepted to characterize voltage mode solutions. IEPE is a *de facto* standard for industrial accelerometers. The IEPE standard offers higher fidelity vibration measurements compared to vibration measurements via a conventional 4–20-mA current loop [13]. There are relatively few IEPE standard solutions for other types of sensors. In particular, IEPE-compatible front-end electronics do not, unfortunately, allow for dc signal transmission.

This article demonstrates an instrumentation and measurement strategy for increasing the compatibility of the IEPE interface to a wider range of sensors. Custom hardware extends the IEPE interface to low-frequency and dc signal transmission via frequency modulation. Following a description of the expanded hardware interface, this article demonstrates the applications for temperature and strain measurements.

Manuscript received October 12, 2020; revised December 27, 2020; accepted January 13, 2021. Date of publication February 3, 2021; date of current version February 25, 2021. This work was supported in part by the Office of Naval Research Structural Acoustics Program and in part by the Fulbright Foundation. The Associate Editor coordinating the review process for this article was Dr. Ferran Reverter. *(Corresponding author: Łukasz Huchel.)*

Łukasz Huchel, Thomas C. Krause, and Steven B. Leeb are with the Department of Electrical Engineering and Computer Science, Massachusetts Institute of Technology, Cambridge, MA 02139 USA (e-mail: lhuchel@mit.edu; tkrause@mit.edu; sbleeb@mit.edu).

Jan Helsen is with OWI-lab/Vrije Universiteit Brussel, 1050 Brussel, Belgium (e-mail: jan.helsen@vub.be).

Digital Object Identifier 10.1109/TIM.2021.3056753

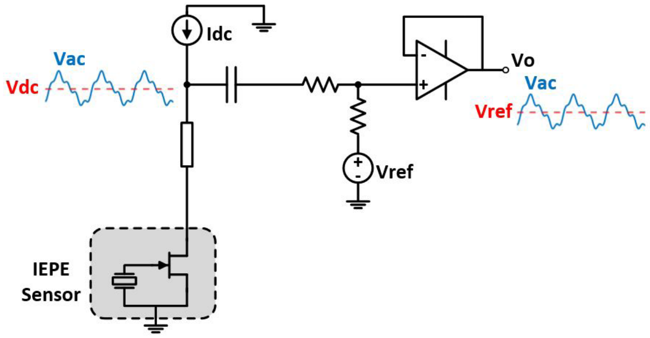

Fig. 1. Typical IEPE interface.

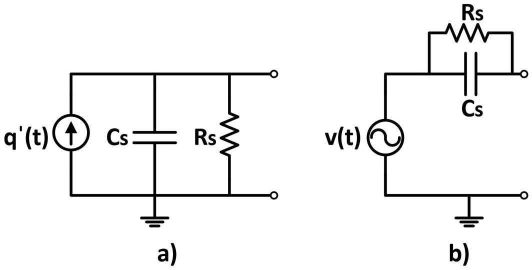

Fig. 2. Piezoelectric circuit models: (a) charge source and (b) voltage source.

In addition, an inexpensive IEPE-compatible microphone is presented. The new sensor interface and microphone are combined with an embedded device to form a condition monitoring system with the ability to implement custom signal processing for different sensing strategies. The embedded device was designed to comply with the requirements of the IEPE interface, as well as, offer remote sensing and "edge" computing. Wireless communication minimizes the installation burden.

II. STANDARD IEPE INTERFACE

IEPE accelerometers have built-in electronics that provide a low-impedance output. They are commonly referred to as (low-impedance) voltage mode/output accelerometers. This type of sensor output does not require low-noise cabling [9]. Standard coaxial cables and connectors such as Bayonet Neill–Concelman Connector (BNC) or SubMiniature version A Connector (SMA) provide great performance at a reasonable cost for many applications. The mechanical features of coaxial cables and connectors provide good shielding for the whole transmission path. Another advantage of this interface is simultaneous power delivery and signal transmission over the same two wires. A typical IEPE interface is shown in Fig. 1.

Two types of amplifiers are employed in the IEPE sensor itself: either discrete FET and bipolar junction transistor (BJT) amplifiers or op-amp-based amplifiers. Typically, only the FET and BJT discrete solutions can benefit from a two-wire interface. Op-amp-based solutions usually involve a three- or four-wire interface [9]. As shown in Fig. 1, a current source provides a dc current component and establishes a dc bias V_{dc} across the impedance of the sensor. This dc bias directly impacts the dynamic range of the sensor [10]. The dynamic range is defined as the ratio between the largest and smallest signal values the sensor can measure. The built-in amplifier sets the sensitivity of the sensor. Other vendor-specific proprietary names, such as ICP, CCLD, IsoTron, or DeltaTron, all refer to the IEPE class of sensors.

In the overall IEPE sensor system, dc bias is removed by an ac coupling capacitor. The ac component V_{ac} of the signal is referred to a common-mode reference voltage V_{ref}, and this allows for a unipolar power supply for the antialiasing filter and upstream analog front end. The ac coupling does not limit the sensing performance, as long as the effective high-pass frequency due to the ac coupling capacitor does not exceed sensor's lowest frequency. The internal properties of a piezoelectric transducer limit available dc information anyway, so the piezoelectric sensor marries well with the IEPE hardware. The piezoelectric material equivalent circuit shown in Fig. 2 [14]–[16] has no excitation if the rate of change of charge is zero, i.e., at static mechanical stress. Limitations on sensor bandwidth are modeled by the resistor and capacitor elements in the circuit model.

III. IEPE TRANSDUCER

Ac coupling does not limit the measurement of vibration or acoustic signatures; however, it limits possible applications of the IEPE interface for measurement of quantities, such as temperature or pressure [11]. Conventionally, other two-wire interfaces can transmit dc measurements but lack the benefits provided by the IEPE interface. A two-wire interface that allows for high-fidelity dc and ac signal transmission, as well as power delivery over the same medium, is of great interest. To address this need, an extension of the IEPE interface is proposed here. This extension enables new measurements to be acquired over the IEPE interface. The new sensor solution utilizes frequency modulation for signal transmission; thus, it presents high-noise immunity [17]. Fig. 3(a) shows possible input connections, i.e., single-ended voltage or Wheatstone bridge configuration. Fig. 3(b) shows a differential amplifier at the transducer input. Fig. 3(c) and (d) shows the power stage and on-board oscillator, respectively.

A. Input Stage, Power Stage, and Amplifier

Fig. 3(a) shows two alternative ways of connecting the sensing element. A passive sensing element with measurand-dependent resistance is commonly used with the Wheatstone bridge configuration. A small resistance R_i is added in series with the Wheatstone bridge to limit current consumption. The series resistance impacts the mapping between sensed voltage V_s and resistance of the sensing element R_s. The mapping of V_s to R_s is given in the following equation:

$$R_s = \frac{V_{cc} R_x^2 - V_s\left(3 R_i R_x + 2 R_x^2\right)}{V_s(R_i + 2R_x) + V_{cc} R_x}. \tag{1}$$

Sensing is not limited to a Wheatstone bridge configuration. Single-ended voltage fed sensing elements can be used as an input to the transducer. Fig. 3(a) shows a TMP35 temperature sensor providing a voltage V_s.

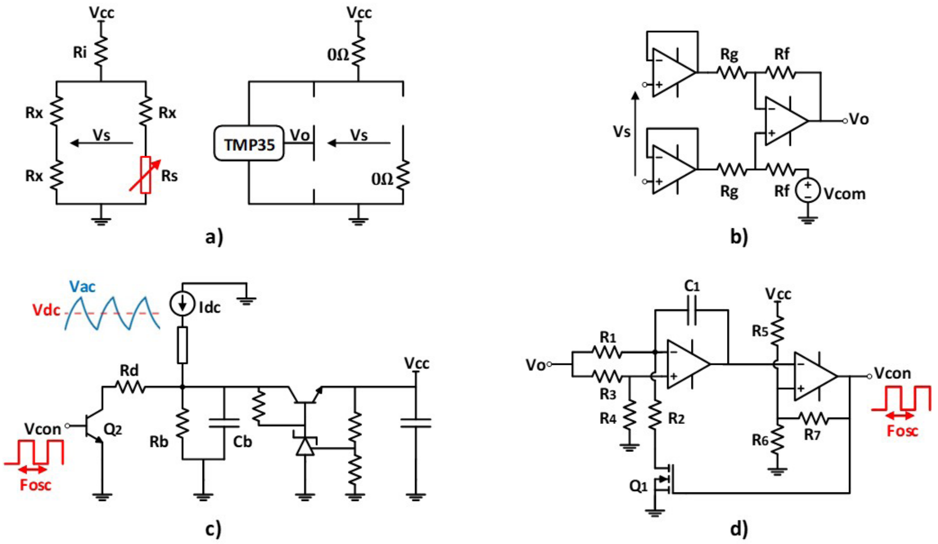

Fig. 3. Structure of the IEPE transducer: (a) input stage, (b) differential amplifier, (c) power stage, and (d) oscillator stage.

In order to accommodate a wide class of input signals, a differential input amplifier with high-input impedance is used. A differential amplifier with input buffers is presented in Fig. 3(b). The amplifier converts a differential signal into a single-ended quantity without loading the Wheatstone bridge stage.

The power stage is shown in Fig. 3(c). It is built around a bias network $R_b||C_b$ and a series regulator. The current source generates a dc bias across the bias network, which is used to generate a stable voltage V_{cc} for on-board electronics.

B. Oscillator Stage

The single-ended control signal, V_o, at the output of the amplifier stage is used as a control input to the oscillator stage of the transducer. It controls the center frequency of the voltage-controlled oscillator. There are several voltage-controlled oscillator solutions for high-frequency applications [17]. However, to limit the burden on the acquisition device, an audio frequency range relaxation oscillator is realized. High-frequency modulation requires very high sampling frequencies or modulation and demodulation techniques, e.g., In-phase (I) and Quadrature (Q) (IQ) modulation. Such a configuration would limit compatibility with many commercial IEPE acquisition devices and, thus, is avoided.

The relaxation oscillator used in the proposed transducer is presented in Fig. 3(d). It consists of an op-amp, comparator, one transistor, and eight passive components. In order to achieve the desired performance, the components around the negative feedback amplifier are designed as follows: $R_3 = R_4$ and $R_1 = 2R_2$. To reflect this and enable further derivations, the oscillator circuit is repeated in Fig. 4, together with necessary node labels and waveform of voltage at node V_z. The input op-amp operates with negative feedback and the voltage at node V_x equals $(1/2)V_o$, i.e., half the control input. To get the relation between input voltage and frequency of the oscillator, the capacitor current $i_{C_1}(t)$ is evaluated in both states of switch Q_1. The high gain of the amplifier and negative feedback leads to expressions for $i_{C_1}^{\mathrm{ON}}(t)$ and $i_{C_1}^{\mathrm{OFF}}(t)$ in terms of the voltage at node V_x

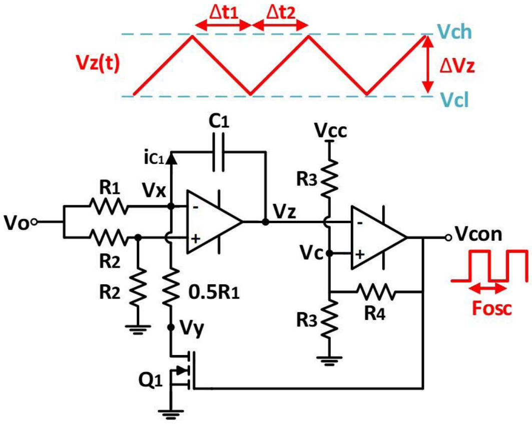

Fig. 4. Oscillator stage.

$$\begin{cases} i_{C_1}^{\mathrm{ON}}(t) = v_x(t)\dfrac{R_{\mathrm{ds}} - 0.5R_1}{R_1(0.5R_1 + R_{\mathrm{ds}})} \\ i_{C_1}^{\mathrm{OFF}}(t) = \dfrac{v_x(t)}{R_1} \end{cases} \tag{2}$$

where R_{ds} is the drain-to-source resistance when MOSFET is turned on. If R_{ds} is neglected, $i_{C_1}^{\mathrm{ON}}(t) = -i_{C_1}^{\mathrm{OFF}}(t)$.

A virtual short assumption does not apply to the output stage comparator inputs because of positive feedback. However, limit values of the voltage at node V_c allow for calculation of the voltage swing across C_1, namely ΔV_z. The limit values at node V_c are marked in Fig. 4 and can be expressed in (3) with the assumption of V_{cc} or ground potential at the output of comparator in saturation

$$\begin{cases} V_{\mathrm{ach}} = V_{cc}\dfrac{R_3}{R_3 + R_3||R_4} \\ V_{\mathrm{cl}} = V_{cc}\dfrac{R_3||R_4}{R_3 + R_3||R_4} \end{cases}. \tag{3}$$

The voltage swing at node V_z is $\Delta V_z = V_{\mathrm{ach}} - V_{\mathrm{cl}}$. The static operating point is considered next, i.e., $v_o(t) = V_o$. Capacitor

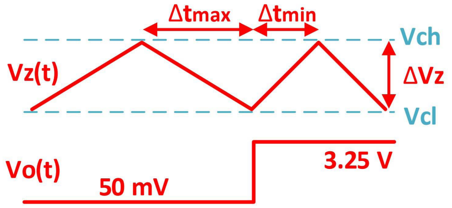

Fig. 5. Transient response of the oscillator.

currents are static in each stage of operation and with R_{ds} neglected are equal to $i_{C_1}^{\mathrm{ON}}(t) = -(0.5V_o/R_1)$ and $i_{C_1}^{\mathrm{OFF}}(t) = (0.5V_o/R_1)$. The charge–voltage relationship of a capacitor is applied, which leads to Δt_1 and Δt_2 as expressed in (4). With a constant input signal, the ac component of the capacitor voltage equals the ac component at node V_z

$$\Delta t_1 = \Delta t_2 = \frac{\Delta V_z C_1}{I_{C_1}} \tag{4}$$

where I_{C_1} equals $|(0.5V_o/R_1)|$. Based on (4), the frequency F_{osc} of the output signal is equal to

$$F_{\mathrm{osc}} = \frac{1}{2\Delta t_1}. \tag{5}$$

The output signal drives the base of transistor Q_2 in Fig. 3(a). The transistor connects a resistor in parallel with the biasing network $R_b||C_b$ and periodically modulates the impedance of the transducer. A dc current source will generate a voltage drop proportional to the instantaneous value of the impedance at the transducer node.

C. Dynamic Performance

The relaxation oscillator may introduce a delay at transients. To quantify the delay, a maximum $\Delta t_{\max}$ and minimum $\Delta t_{\min}$ are evaluated with (4). The input signal V_o can be between 0.05 and 3.25 V (with $V_{cc} = 3.3\ V$), and at zero response, it equals V_{com} [see Fig. 3(b)]. In the realized sensor, the voltage swing ΔV_z across the feedback capacitor C_1 is equal to 1.775 V. Assuming the maximum change of the control signal from 0.05 to 3.25 V, the feedback capacitor current changes from 0.58 to 37.8 μA based on (2) ($R_1 = 43$ kΩ and $C_1 = 470$ pF). Assuming a transient in the input signal presented in Fig. 5 and following (4), the maximum period deviation $|\Delta t_{\max} - \Delta t_{\min}|$ is 1.4 ms. In the next cycle, the oscillator resumes the correct frequency. The extreme change of the control signal from 50 mV to 3.25 V corresponds to a step change across the full range of the measured quantity (see Fig. 5). In practice, all physical phenomena have limited bandwidth and a step change is very exaggerated. A more realistic bound on input signal bandwidth is considered. The input impedance R_s is varied between 100 Ω and 70 kΩ, while R_i and R_x in the bridge in Fig. 3(a) are equal to 499 Ω and 1 kΩ, respectively. With an amplifier stage of gain 0.5, the input voltage of the oscillator circuit ranges from 1.20 to 2.24 V. Considering (2)–(5), the frequency range is given in Fig. 6. The oscillator frequency varies between 8.02 and 14.93 kHz. The maximum frequency of the input signal is constrained to less than approximately 10% of the minimum oscillator frequency. Thus, the input signal frequency content should not exceed 1 kHz. For a typical thermistor characteristic, the considered range of input resistance corresponds to a wide temperature range between −55 °C and 90 °C [18]. The oscillator frequency is limited by the Nyquist rate of the IEPE acquisition device. Higher sampling frequency enables increased oscillator frequency and thus higher input signal bandwidth.

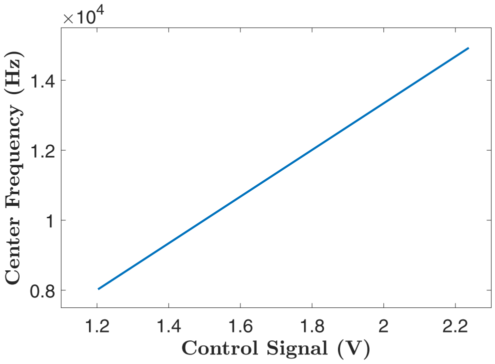

Fig. 6. Oscillator frequency as a function of input voltage.

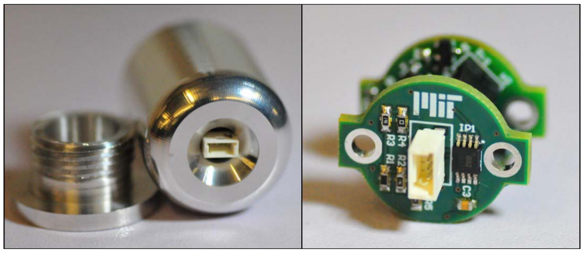

Fig. 7. Proposed IEPE transducer and custom aluminum case.

All four stages described above enable a wide range of measurements over the IEPE interface. The oscillator stage encodes the instantaneous value of the input signal, either from the Wheatstone bridge or a single-ended voltage source, into an output voltage frequency. The sensing configuration presented in Fig. 3(a) enables two-wire measurements of sensors that in general require at least three wires, i.e., V_{cc}, ground and output signal. In addition, the conversion of sensing element properties into an electrical quantity, i.e., transduction, can happen very close to the system under study. The proposed transducer reduces the length of the connection between a high-impedance sensing element and transducing element. Consequently, the noise immunity is improved. The transducer output is transmitted with a standard coaxial cable and BNC or SMA connector technology, simplifying cable management. The transducer is shown in Fig. 7. A stack of two printed circuit boards was used for a cylindrical transducer shape. The aluminum case provides external protection and EMI shielding. Once assembled, only the input and SMA connectors are exposed.

IV. APPLICATIONS OF THE IEPE TRANSDUCER

The IEPE transducer was tested with several sensing elements. In this section, example applications with a negative temperature coefficient (NTC) thermistor and strain gauge are presented. A sensitivity analysis describes the sensor performance in more detail.

A. Sensitivity Analysis

Modern digital acquisition systems can handle a wide range of sensor nonlinearity; however, a linear transducer response is desired [11]. Equation (4) and Fig. 6 show that the amplifier and oscillator stages present the desired linearity. Despite the linearity of the amplifier and oscillator stages, the mapping from sensing element signal to its resistance is nonlinear [see (1)]. However, this is a feature of the Wheatstone bridge and not the proposed topology. If a voltage source sensing element is used, as shown in Fig. 3(c), linearity is preserved.

The frequency of the output signal is expressed in (6), see Fig. 3 for circuit details

$$F_{\mathrm{osc}} = \frac{\frac{V_{\mathrm{com}} - V_s\left(\frac{R_f}{R_g}\right)}{2R_1}}{2\Delta V_z C_1}. \tag{6}$$

The sensitivity analysis based on (6) provides insight into oscillator frequency error due to variations in component values. Equation (7) provides the expressions for the relative error of oscillator frequency

$$\begin{cases} S_{C_1} = \dfrac{C_1}{F_{\mathrm{osc}}}\dfrac{\delta F_{\mathrm{osc}}}{\delta C_1} = C_1 \Delta V_z C_1 \\ \qquad \cdot \left(\dfrac{1}{I_{C_1}^{\mathrm{ON}}} + \dfrac{1}{I_{C_1}^{\mathrm{OFF}}}\right)\dfrac{-1}{\Delta V_z C_1^2\left(\frac{1}{I_{C_1}^{\mathrm{ON}}} + \frac{1}{I_{C_1}^{\mathrm{OFF}}}\right)} = -1 \\ S_{R_f} = \dfrac{R_f}{F_{\mathrm{osc}}}\dfrac{\delta F_{\mathrm{osc}}}{\delta R_f} = 1 \\ S_{R_g} = \dfrac{R_g}{F_{\mathrm{osc}}}\dfrac{\delta F_{\mathrm{osc}}}{\delta R_g} = -1 \end{cases}. \tag{7}$$

Equation (2) was derived under assumption of ideal matching between resistor values. In general, the voltage at node V_x will deviate if the resistors R_2 in Fig. 4 are not matched. Component labels from Fig. 3(d) are used in the formulas mentioned in the following:

$$\begin{cases} S_{R_1} = \dfrac{R_3R_4R_1}{R_3R_4R_1 - R_3^2R_2} - 2 \\ S_{R_2} = -\dfrac{R_3R_2}{R_4R_1 - R_3R_2} \\ S_{R_3} = \dfrac{R_4R_1 - 2R_3R_2}{R_1R_4 - R_3R_2} - \dfrac{R_3}{R_3 + R_4} \\ S_{R_4} = \dfrac{R_4R_1}{R_4R_1 - R_3R_2} - \dfrac{R_3 + 2R_4}{R_3 + R_4} \\ S_{R_5} = -\dfrac{R_6R_7}{R_5R_6 + R_5R_7 + R_6R_7} \\ S_{R_6} = -\dfrac{R_5R_7}{R_5R_6 + R_5R_7 + R_6R_7} \\ S_{R_7} = \dfrac{R_7(R_6 + R_5)}{R_5R_6 + R_5R_7 + R_6R_7} \end{cases}. \tag{8}$$

When $R_3 = R_4$ and $R_2 = 0.5R_1$, the sensitivities have the following values: $S_{R_1} = 0$, $S_{R_2} = -1$, $S_{R_3} = -0.5$, and $S_{R_4} = 0.5$. Expressions for S_{R_5}, S_{R_6}, and S_{R_7} depend on the particular circuit implementation, and with the designed circuit parameters, S_{R_5}, S_{R_6}, and S_{R_7} have the following values: $S_{R_5} = -0.23$, $S_{R_6} = -0.23$, and $S_{R_7} = 0.4624$.

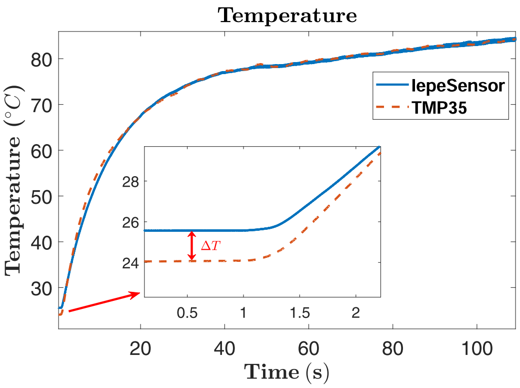

Fig. 8. Temperature measurement comparison.

For uncorrelated errors, the total mean square error of the oscillator frequency is due to the variations in component values that are given in (9). High-precision and high thermal stability components should be used to minimize error, e.g., ceramic capacitors with C0G dielectric and 0.1% tolerance resistors. For 0.1% tolerance resistors and a 1% tolerance capacitor, the total mean square error of oscillator frequency is 1.02%. Thus, the frequency error for the oscillator in Fig. 4 is driven mostly by the deviation in capacitance value, $S_{F_{\mathrm{osc}}} \approx S_{C_1}$. Commonly available C0G ceramic capacitors in the range of 500 pF are typically only offered with tolerance above 1%

$$S_{F_{\mathrm{osc}}} = \left(S_{C_1}^2\delta_{C_1}^2 + S_{R_f}^2\delta_{R_f}^2 + S_{R_g}^2\delta_{R_g}^2 + \sum_{n=1}^{7} S_{R_n}^2\delta_{R_n}^2\right)^{\frac{1}{2}}. \tag{9}$$

δ in (9) is a standard deviation of value of each component.

B. IEPE Temperature Sensor

Temperature sensing is an example application of the new measurement solution. A conventional NTC thermistor is used as a sensing element R_s [see Fig. 3(a)]. The resistance of the sensing element varies between 40 Ω and 70 kΩ throughout its operating range. A TMP35 temperature sensor was used as a reference. Both the NTC thermistor and TMP35 sensor have similar packaging and dimensions; thus, the impact of different dynamics of the sensing elements is neglected in the comparison. Fig. 8 shows the reference measurement and the response of IEPE temperature transducer. Data presented in Fig. 8 were acquired without calibration of the transducer, and (1)–(5) were used to convert frequency into the resistance of the sensing element.

A very good dynamic response can be seen in Fig. 8. The steady-state response shows a good match with the reference temperature profile. The temperature deviation ΔT is equal to 1.5 °C. This is less than the accuracy of TMP35 [19], which is ±2 °C.

C. IEPE Strain Gauge

Another application presented in this article is measurement with a strain gauge. A conventional Wheatstone bridge can

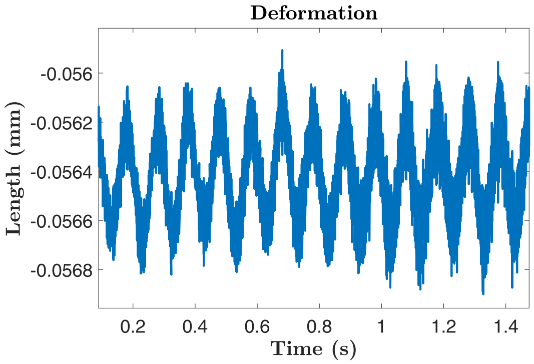

Fig. 9. Strain measurement.

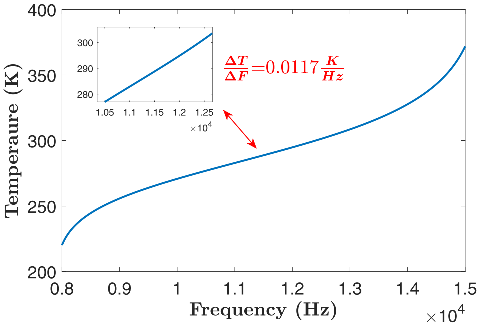

Fig. 10. Temperature as a function of oscillator frequency.

be supplied by either a voltage [Fig. 3(a)] or current source. The current source configuration should not be confused with the proposed current loop transducer. There are a few market solutions offered as IEPE strain gauges, such as model 740B02. Available solutions have a nonzero cutoff frequency in the low range [20], i.e., the transducer is not able to measure static or very slowly varying phenomena. In the case of a strain gauge, this could be a static strain on the monitored structure. As demonstrated with temperature, the ability to perform static measurements is a key feature of the proposed solution. A strain gauge with 3.5-kΩ nominal resistance and gauge factor of two was used in the test. The strain gauge was attached to a subwoofer membrane to allow for a controllable excitation frequency. The response of the IEPE strain gauge measurement to a 10-Hz excitation is presented in Fig. 9. The offset in the data in Fig. 9 corresponds to the static deformation of the strain gauge due to the natural curvature of the membrane.

D. Transducer Output Processing

The output of the IEPE transducer is a continuous frequency-modulated voltage waveform. As described in Section IV-A, the accuracy of the transducer output is determined by component tolerances. However, the method used to process the transducer output can introduce finite measurement resolution. The output is processed in real time or recorded and processed offline. For example, in an offline analysis, the Hilbert transform is applied for instantaneous phase angle and frequency calculation. A frequency estimate is mapped to the measurement domain with (1)–(6). In such a configuration, resolution is not a concern. However, the Hilbert transform is noncausal and is not suited for real-time processing. In real-time applications, comment on processing resolution is necessary.

Real-time processing is investigated with temperature measurement used as an example. In a particular circuit realization, the transducer output has a fundamental frequency of 15.4 kHz for a sensing resistance of $R_s = 0\ \Omega$ at the input stage. An output with a fundamental frequency of 8.02 kHz corresponds to a sensing resistance of $R_s = 70$ kΩ. For the NTC thermistor described in [18], this range of resistance covers temperatures between −55 °C and 125 °C. The temperature, T, is plotted as a function of frequency, F, in Fig. 10. Due to the characteristic of the thermistor, the mapping is nonlinear. One candidate for accurate real-time frequency estimation is the time-dependent discrete Fourier transform (DFT). However, a finite length DFT imposes limits on frequency resolution ΔF. To provide a quantitative measure of the impact of DFT frequency resolution on temperature sensing, the DFT of length 32 768 is considered for data sampled at a rate of 48 kHz. In this case, ΔF equals 1.46 Hz, i.e., the abscissa of Fig. 10 is discretized in increments of 1.46 Hz. Due to the nonlinear nature of the characteristic in Fig. 10, the temperature resolution varies with frequency. From 10 to 13 kHz, the temperature-frequency characteristic is well approximated as linear. Within this region and with the assumed DFT resolution $\Delta F = 1.46$ Hz, the temperature resolution is $\Delta T \approx 0.017$ °C.

In this section, the detailed analysis reveals that the magnitude of all IEPE transducer sensitivity coefficients $|S|$ is less than or equal to one. The dominant component of output frequency error is due to the feedback capacitor in the oscillator stage. Two example applications of the IEPE transducer were investigated. Both the thermistor and strain gauge measurements demonstrated a successful extension of the IEPE interface.

V. IEPE MICROPHONE

Microphones are characterized by the principle of transduction. They convert acoustic waves into electrical signals. Microphones are used in settings ranging from musical performance to electromechanical system diagnostics [21], [22]. The most common types of microphones are dynamic, piezoelectric, condenser, and electret microphones. Dynamic microphones use a moving coil for transduction, piezoelectric microphones use the piezoelectric effect, and condenser and electret microphones use capacitance variations. Each technology requires a specific amplifier topology [23]. For example, condenser microphones offer high sensitivity and good frequency response; however, they require a high-voltage source to polarize the sensing element and thus have limited application in embedded devices. Sensing elements built with piezoelectric or electret materials do not require polarization circuitry and are conducive to compact sensing solutions [23].

Acoustic signature enables a wide range of diagnostics [24], [25]. A two-wire interface providing excellent shielding is beneficial in noisy industrial environments. IEPE-compatible microphones provide these benefits to the acquisition of

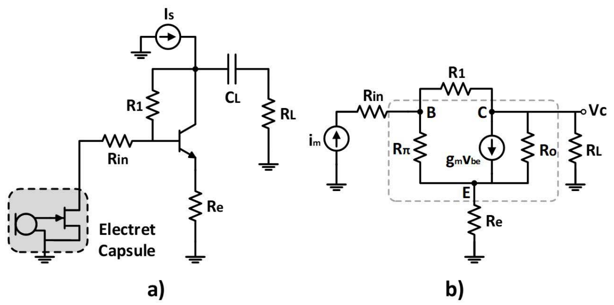

Fig. 11. IEPE microphone: (a) large-signal model and (b) small-signal model.

acoustic signals. There are a few vendors offering IEPE microphones, and some of the available solutions are referred to as constant current power (CCP) microphones [26].

The IEPE class of microphones is characterized by very high cost. A typical price starts around \$500, and much more expensive models are available. These high-end microphones provide excellent performance for critical applications; however, there is a wide range of monitoring applications where high cost is prohibitive. A much cheaper and still reliable IEPE microphone is of great interest. To the best of authors' knowledge, an inexpensive IEPE microphone solution is lacking. In addition, it is very hard to get detailed information on the in-built electronics of IEPE-compatible sensors. The sparse literature presents simplified schematics that do not allow for full comparison or [9]. A reference that discusses affordable current loop microphones is [27]. Although not a scientific reference, it highlights the need for an affordable IEPE microphone and discusses an example implementation.

A low-cost IEPE-compatible microphone that utilizes an electret capsule is presented in this section. It employs a current-fed common emitter amplifier with emitter resistance as a preamplifier stage. A small-signal analysis provides a gain expression that matches experimental results. The schematic of the proposed circuit is shown in Fig. 11(a). A key benefit of this implementation is significantly lower cost when compared to available market solutions. The proposed microphone is not introduced to replace very high-end and expensive market solutions but is meant to enable monitoring for applications where very high instrumentation cost is prohibitive.

The dc operating point is evaluated to calculate the transconductance parameter g_m, which is necessary for the small-signal model of the bipolar transistor. The transconductance parameter is expressed as $g_m = (I_c/V_T)$, where I_c is the collector bias current and V_T is the thermal voltage. To calculate the bias current, the load coupling capacitor C_L in Fig. 11(a) is open and electret capsule is modeled with resistance R_{ds}. At static condition, the microphone can be modeled with resistance because of the output JFET stage inside the electret capsule [23]. The formula for I_c is given in (10). The bias current calculated with (10) matches the dc analysis of the circuit in the SPICE simulator

$$I_c = \alpha \frac{R'_{\mathrm{in}} I_s - V_{\mathrm{be}}}{R_e + R'_{\mathrm{in}}} \tag{10}$$

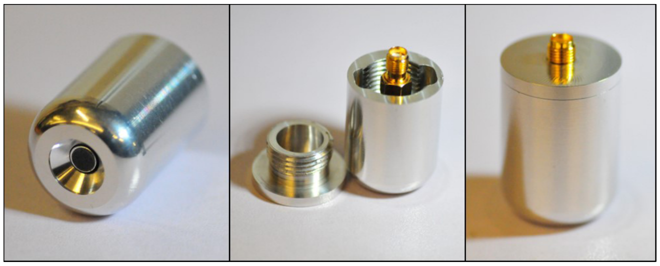

Fig. 12. IEPE microphone and custom aluminum case.

where R'_{in} is the sum of R_{ds} and R_{in}, V_{be} is the base–emitter voltage in the active region of operation ($V_{\mathrm{be}} \approx 0.7$ V), and α is the bipolar transistor current gain parameter.

The small-signal model of the BJT transistor allows for analytical evaluation of amplifier gain. The electret capsule with in-built JFET is considered in the design. The capsule output is modeled as a current source. The complete small-signal circuit is presented in Fig. 11(b). The gain of this circuit is expressed as $G = (v_C/i_m)$, and a detailed expression is provided in (12) in the appendix. The designed circuit has a gain of 75 dB. The employed electret capsule has a sensitivity parameter of $S_i = 8.08$ (μA/Pa) [28], [29]. A 300-Hz harmonic source generated an 83-dB sound pressure level (SPL) measured at the capsule to validate the performance. The output signal, after rejecting dc bias voltage, presented a 45-mV peak value. The estimate of the peak output voltage V_o based on the derived gain and input SPL is given in the following equation:

$$V_o = S_i \cdot G \cdot \mathrm{SPL}_{\mathrm{peak}} = 19 \text{ mV} \tag{11}$$

where SPL of 83 dB is converted to 0.282 Pa and peak SPL value was calculated with a crest factor for sine wave. The electret capsule has a ±4-dB tolerance [28], and thus, the output estimate can range up to 30 mV. In addition, the microphone case alters SPL in comparison to the SPL meter used to set the experimental reference value of 83 dB. All considered, the estimated peak value closely matches the experimental results. The IEPE microphone is shown in Fig. 12.

To verify the performance of the developed IEPE microphone, a total harmonic distortion (THD) comparison with a microphone that utilizes a transimpedance amplifier is presented. The transimpedance amplifier is a widely accepted solution to interface with prepolarized sensing elements [23], [29], such as an electret capsule. In the experiment, the SPL at the electret capsule was held constant at 72 dB for all considered frequencies. Both systems, i.e., IEPE and transimpedance amplifiers, worked with the same model of electret capsule. The THD for both types of amplifiers is presented in Fig. 13, and the microphone with the transimpedance amplifier is denoted as a voltage microphone. To further characterize the IEPE microphone, a sensitivity plot is presented in Fig. 14. The sensitivity data are presented for two SPL values corresponding to 72 dB and the standard 94 dB.

The proposed circuitry provides good performance with a low-cost electret capsule. The IEPE microphone provided essentially the same THD as a common solution.

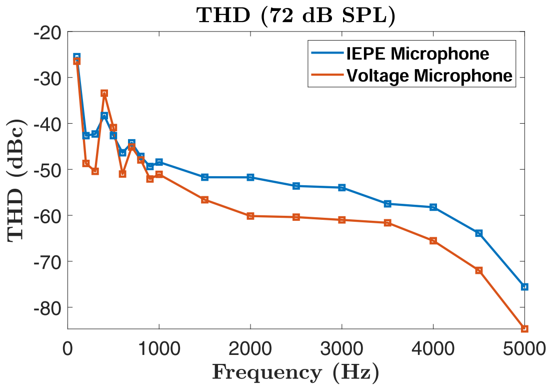

Fig. 13. Microphone THD comparison.

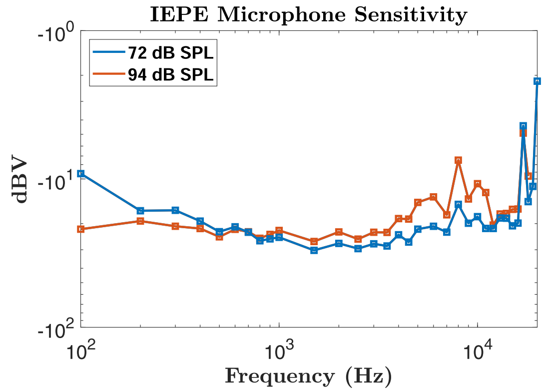

Fig. 14. Microphone sensitivity plot.

The analytical expression for circuit gain closely matches the experimental results.

VI. New Sensing Strategy

Condition monitoring systems provide information about the health of critical components. Reliable, modular, and minimally intrusive condition monitoring systems are of interest to a variety of disciplines. Each measured signal plays a role in condition monitoring. Vibration, acoustic signature, temperature, strain, pressure, and other types of signals all help to evaluate the operating status and condition of systems. The diversity of measurands leads to proprietary connectors, expensive hardware, and interface-specific amplifiers. These constraints increase the complexity and cost of instrumentation for condition monitoring. The stretched abilities of the IEPE interface presented in Sections III and V simplify the necessary hardware for condition monitoring. Paired with an acquisition device, the ensemble forms a compact, versatile, and cost-friendly IEPE-based monitoring solution. A custom wireless data acquisition device is presented in Figs. 15 and 16. It consists of two printed circuit boards that overcome the challenges of mixed analog, digital, and RF domains. The IEPE front-end block in Fig. 16 refers to the IEPE interface circuitry shown in Fig. 1. An example of the suggested monitoring solution is presented in Fig. 17.

A. Acquisition Device

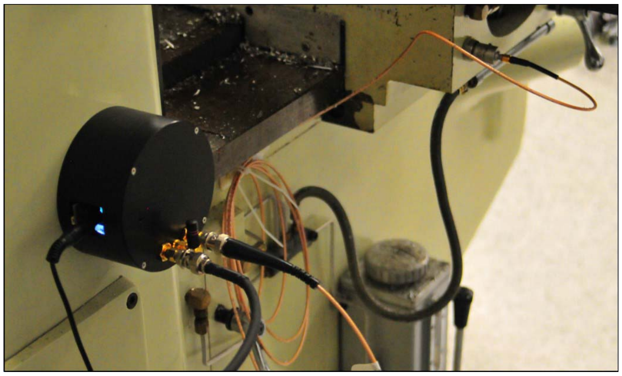

Fig. 15. Data acquisition device (left) with accelerometer (top right).

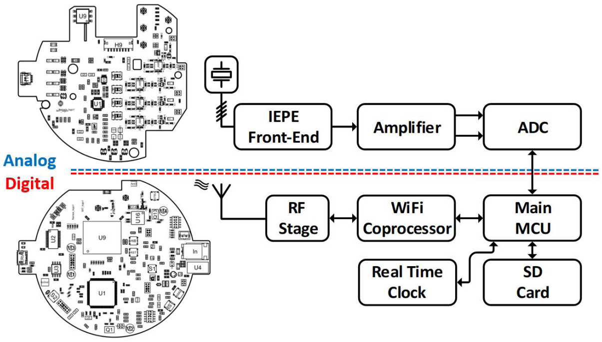

Fig. 16. Block diagram of the device architecture.

Custom acquisition hardware is proposed as a component of a system-level condition monitoring solution. The wireless device offers remote processing power and nonvolatile memory for selective measurement and storage of raw time-series sensor data.

The custom instrumentation offers benefits in data acquisition, detection, and nonintrusive sensing. There are four simultaneously sampled differential channels that are IEPE-compatible. Nonvolatile memory and a real-time clock enable a lightweight data management system. Files are stored using the standard file allocation table (FAT) file system to comply with most modern operating systems. The device operates as a server, and clients can check files in the remote memory, download files, delete files, and ask for new data to be acquired.

The custom instrumentation offers several advantages. A comparison of IEPE microphone measurements performed with the presented device and an IEPE acquisition platform built according to the guidelines in [30] is shown in Fig. 18. As previously described, IEPE devices are excited by a dc current source. The comparison presented in Fig. 18 reveals that the current source implementation of the reference design introduces significant high-frequency noise into measurements. The noise contribution is significant and has a visible effect on signals even in the time-domain representation.

The results shown in Fig. 18 present sampled acoustic signals emitted by a speaker excited at a pure tone. The noisy measurement from the reference hardware is shown in blue, and a measurement from the custom instrumentation is shown in red. Both measurements were performed with the same sampling frequency and bit resolution.

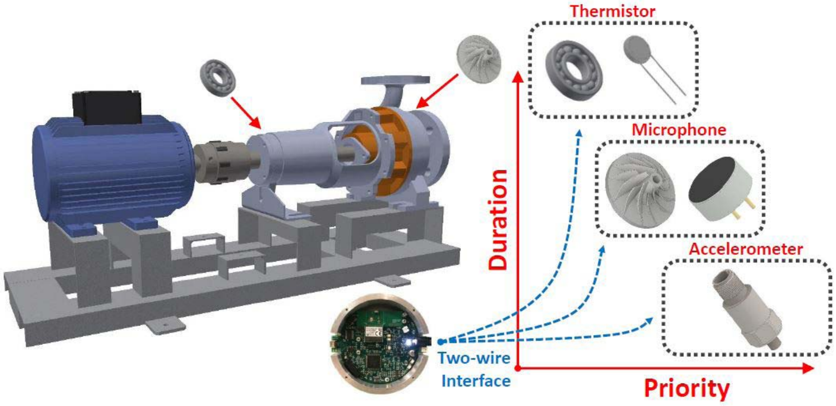

Fig. 17. Proposed sensing strategy in an example scenario.

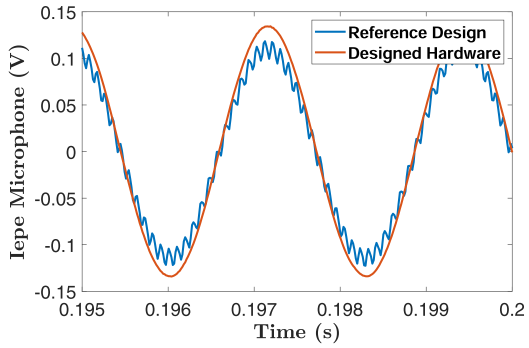

Fig. 18. Sample acoustic signal.

B. Condition Monitoring System Solution

Small footprint, IEPE compatibility, and wireless communication of the proposed device facilitate a general condition monitoring system. Measurements for predictive maintenance are taken throughout the life cycle of equipment. In some cases, the most illustrative condition indicators arise from a measurement of a specific physical operation or phenomenon, e.g., the spin down of rotating machinery [31]. Measurements for predictive maintenance are classified as short duration, high priority. In contrast, measurands, such as temperature and pressure, are continually monitored and classified as long duration but low priority for predictive maintenance. The idea of measurement priority is central to the proposed condition monitoring system. Physical processes with different timescales introduce a natural measurement hierarchy. Natural order can be leveraged for device resource distribution. Variables with low predictive maintenance priority, such as temperature, are very valuable as low-latency alarm criteria, e.g., an overheating bearing can be directly signaled as abnormal. A high-level demonstration of the system with a motor-pump setup is given in Fig. 17. The wireless device, equipped with transducers, microphones, and accelerometers, can coordinate various measurements through a small number of IEPE channels. Natural timescales permit time sharing of the IEPE channels and increase effective channel count. The sensor selection can be done through a digital multiplexer and programmed remotely.

VII. CONCLUSION

IEPE sensing solutions and a condition monitoring system have been developed in this article. A novel IEPE transducer extends the measurement ability of the IEPE interface to slowly varying and dc signals. The IEPE transducer uses a voltage-controlled oscillator to encode signal amplitude to frequency. The sensitivity and bandwidth of the hardware are considered. The performance of the transducer with temperature and strain sensing elements is demonstrated. An IEPE microphone is also considered in this article. A small-signal analysis provides a gain expression that closely matches experimental results. A THD comparison with a microphone that uses a transimpedance amplifier and sensitivity characterizes the performance of the proposed microphone. A condition monitoring system combines the developed instrumentation to create a flexible platform for industrial monitoring. The system enables a variety of measurements with limited device complexity and low overall cost.

APPENDIX

$$\frac{v_C}{i_m} = \frac{AR_o(1-g_mR_1)+(R_1+R_\pi)B}{C-R_oD-(R_1+R_\pi)E} \tag{12}$$

where

$$\begin{aligned}
A &= R_1R_\pi + \frac{R_1^2R_\pi(1+g_mR_\pi)}{a+c}\\
B &= \frac{R_1R_\pi(1+g_mR_\pi)(g_mR_1R_o+R_1)}{a+c}\\
C &= b(R_1+R_\pi)\\
D &= (1-g_mR_1)\left(R_\pi+\frac{R_1a}{a+c}\right)\\
E &= (g_mR_1R_o+R_1)\frac{a}{a+c}\\
a &= (1+g_mR_\pi)R_\pi+\frac{R_\pi+R_1}{R_o}R_\pi\\
b &= \frac{R_oR_L+R_oR_1+R_LR_1}{R_L}\\
c &= \frac{R_\pi+R_1}{R_e}R_\pi.
\end{aligned}$$

REFERENCES

[1] P. Ferrari, A. Flammini, E. Sisinni, S. Rinaldi, D. Brandão, and M. S. Rocha, "Delay estimation of industrial IoT applications based on messaging protocols," *IEEE Trans. Instrum. Meas.*, vol. 67, no. 9, pp. 2188–2199, Sep. 2018.

[2] L. Angrisani, P. Arpaia, A. Esposito, and N. Moccaldi, "A wearable brain–computer interface instrument for augmented reality-based inspection in industry 4.0," *IEEE Trans. Instrum. Meas.*, vol. 69, no. 4, pp. 1530–1539, Apr. 2020.

[3] G. D'Emilia, A. Gaspari, and E. Natale, "Mechatronics applications of measurements for smart manufacturing in an industry 4.0 scenario," *IEEE Instrum. Meas. Mag.*, vol. 22, no. 2, pp. 35–43, Apr. 2019.

[4] D. Kong, Y. Chen, N. Li, C. Duan, L. Lu, and D. Chen, "Tool wear estimation in end milling of titanium alloy using NPE and a novel WOA-SVM model," *IEEE Trans. Instrum. Meas.*, vol. 69, no. 7, pp. 5219–5232, Jul. 2020.

[5] J.-H. Zhou, C. K. Pang, Z.-W. Zhong, and F. L. Lewis, "Tool wear monitoring using acoustic emissions by dominant-feature identification," *IEEE Trans. Instrum. Meas.*, vol. 60, no. 2, pp. 547–559, Feb. 2011.

[6] L. Zhang, R. X. Gao, and K. B. Lee, "Spindle health diagnosis based on analytic wavelet enveloping," *IEEE Trans. Instrum. Meas.*, vol. 55, no. 5, pp. 1850–1858, Oct. 2006.

[7] W. Altmann, D. Macdonald, and S. Mackay, *Practical Process Control for Engineers Technicians*. Oxford, U.K.: Newnes, 2005. [Online]. Available: http://www.sciencedirect.com/Pscience/article/pii/B9780750664004500021

[8] S. Gill. (Apr. 2013). *HART: Benefits for Today and Into the Future*. [Online]. Available: https://www.controleng.com/articles/hart-benefits-for-today-and-into-the-future/

[9] F. Levinzon, *Piezoelectric Accelerometers With Integral Electronics*. Cham, Switzerland: Springer, 2015.

[10] J. Lally, "Accelerometer selection considerations charge and ICP integrated circuit piezoelectric," PCB Piezotronics, Inc. Depew, NY, USA, Tech. Note TN-17, 2005.

[11] G. Gautschi, *Piezoelectric Sensorics: Force, Strain, Pressure, Acceleration and Acoustic Emission Sensors, Materials and Amplifiers*. Heidelberg, Germany: Springer, 2002.

[12] F. A. Levinzon, "Ultra-low-noise seismic piezoelectric accelerometer with integral FET amplifier," *IEEE Sensors J.*, vol. 12, no. 6, pp. 2262–2268, Jun. 2012.

[13] *VibraSens*. Accessed: 2020. [Online]. Available: https://www.vibrasens.com/4-20-ma/

[14] K. Kanda, T. Saito, Y. Iga, K. Higuchi, and K. Maenaka, "Influence of parasitic capacitance on output voltage for series-connected thin-film piezoelectric devices," *Sensors*, vol. 12, pp. 16673–16684, Dec. 2012.

[15] J. Karki, "Signal conditioning piezoelectric sensors," Texas Instrum., Dallas, TX, USA, Appl. Rep. SLOA033A, 2000.

[16] M. Serridge and T. R. Llcht, "Piezoelectric accelerometers and vibration preamplifiers," in *Bruel&Kjaer Theory and Application Handbook*. Nærum, Denmark: Brüel & Kjær Handbook, 1987.

[17] A. S. Sedra and K. C. Smith, *Microelectronic Circuits*, 5th ed. New York, NY, USA: Oxford Univ. Press, 2007.

[18] *NTC Thermistors for Temperature Measurement Leaded NTC Thermistors, Lead Spacing 5 mm*, TDK, Tokyo, Japan, Jan. 2018.

[19] *Low Voltage Temperature Sensors; Data Sheet TMP35/TMP36/TMP37*, Analog Devices, Norwood, MA, USA, 2013.

[20] *Reuseable Piezoelectric ICP Strain Sensor; SERIES 740XXX*, PCB Piezotronics, Depew, NY, USA, 2019.

[21] J. Bordoy, C. Schindelhauer, F. Höflinger, and L. M. Reindl, "Exploiting acoustic echoes for smartphone localization and microphone self-calibration," *IEEE Trans. Instrum. Meas.*, vol. 69, no. 4, pp. 1484–1492, Apr. 2020.

[22] J. Kranjec, S. Beguš, J. Drnovšek, and G. Geršak, "Novel methods for noncontact heart rate measurement: A feasibility study," *IEEE Trans. Instrum. Meas.*, vol. 63, no. 4, pp. 838–847, Apr. 2014.

[23] T. Starecki, "Analog front-end circuitry in piezoelectric and microphone detection of photoacoustic signals," *Int. J. Thermophys.*, vol. 35, pp. 1–16, Nov. 2014.

[24] J. Cui and Z. Li, "Synchronous 3-D imaging and velocity estimation of underwater targets using pulse-pair acoustical imaging technique," *IEEE Trans. Instrum. Meas.*, vol. 69, no. 8, pp. 5369–5384, Aug. 2020.

[25] F. J. Alvarez, T. Aguilera, J. A. Paredes, and J. A. Moreno, "Acoustic tag identification based on noncoherent FSK detection with portable devices," *IEEE Trans. Instrum. Meas.*, vol. 67, no. 2, pp. 270–278, Feb. 2018.

[26] *Product Catalogue Measurement Microphones Q1-2020*, GRAS Sound Vib., Holte, Denmark.

[27] R. Elliott. (2011). *4mA Current Loop Microphone System*. [Online]. Available: https://sound-au.com/project134.htm

[28] *POM-3535P-3-R Microphone*, PUI Audio, Dayton, OH, USA, 2013.

[29] J. Caldwell, "Single-supply, electret microphone pre-amplifier reference design," Texas Instrum., Dallas, TX, USA, Appl. Rep. TIDU765, 2015.

[30] A. Noeman, "IEPE vibration sensor interface reference design for PLC analog input," Texas Instrum., Dallas, TX, USA, Appl. Rep. TIDA-01471, 2017.

[31] R. Zachar, P. Lindahl, J. Donnal, W. Cotta, C. Schantz, and S. B. Leeb, "Utilizing spin-down transients for vibration-based diagnostics of resiliently mounted machines," *IEEE Trans. Instrum. Meas.*, vol. 65, no. 7, pp. 1641–1650, Jul. 2016.

Łukasz Huchel received the B.Sc. degree in electrical power engineering from the Silesian University of Technology, Gliwice, Poland, in 2013, and the M.Sc. degree from the Department of Electrical Engineering and Computer Science (EECS), Masdar Institute of Science and Technology, Abu Dhabi, United Arab Emirates, in 2015. He is currently pursuing the Ph.D. degree in EECS with the Massachusetts Institute of Technology, Cambridge, MA, USA.

His current research interests include the development of signal processing algorithms, and hardware and software solutions for condition monitoring and diagnostics.

Thomas C. Krause received the B.S. degree in electrical engineering from Purdue University, West Lafayette, IN, USA, in 2019. He is currently pursuing the Ph.D. degree in electrical engineering and computer science with the Massachusetts Institute of Technology, Cambridge, MA, USA.

His current research interests include the development of signal processing algorithms and sensors for energy and condition monitoring.

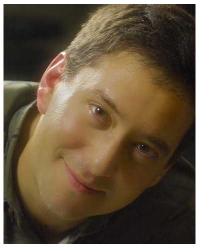

Steven B. Leeb (Fellow, IEEE) received the Ph.D. degree from the Massachusetts Institute of Technology (M.I.T.), Cambridge, MA, USA, in 1993.

He has authored or coauthored more than 200 publications and 20 U.S. patents in the fields of electromechanics and power electronics.

Dr. Leeb has served as a Commissioned Officer in the U.S. Air Force (USAF) reserves, and he has been a member of the M.I.T. Faculty with the Department of Electrical Engineering and Computer Science since 1993. He also holds a joint appointment at MIT's Department of Mechanical Engineering.

Jan Helsen received the M.Sc. degree in electromechanical engineering and the Ph.D. degree from Katholieke Universiteit Leuven, Leuven, Belgium, in 2007 and 2012, respectively. His Ph.D. thesis was focused on the dynamic simulation of wind turbine gearboxes.

He is currently a Professor with the Acoustics and Vibrations Research Group, Vrije Universiteit Brussel, Brussel, Belgium. His current research interest includes condition monitoring of rotating systems.